2012-10-01

Epigenetic control of cell cycle-dependent histone gene expression is a principal component of the abbreviated pluripotent cell cycle

Ricardo F. Medina
University of Massachusetts Medical School

Et al.

MCB
Journals.ASM.org

Epigenetic Control of Cell Cycle-Dependent Histone Gene Expression Is a Principal Component of the Abbreviated Pluripotent Cell Cycle

Ricardo Medina,[a] Prachi N. Ghule,[a] Fernando Cruzat,[b] A. Rasim Barutcu,[a] Martin Montecino,[c] Janet L. Stein,[a]* Andre J. van Wijnen,[a] and Gary S. Stein[a]*

Department of Cell Biology and Cancer Center, University of Massachusetts Medical School, Worcester, Massachusetts, USA[a]; Department of Biochemistry and Molecular Biology, Faculty of Biological Sciences, Universidad de Concepción, Concepción, Chile[b]; and Centro de Investigaciones Biomédicas, Facultad de Ciencias Biológicas y Facultad de Medicina, Universidad Andrés Bello, Santiago, Chile[c]

Self-renewal of human pluripotent embryonic stem cells proceeds via an abbreviated cell cycle with a shortened G_1 phase. We examined which genes are modulated in this abbreviated period and the epigenetic mechanisms that control their expression. Accelerated upregulation of genes encoding histone proteins that support DNA replication is the most prominent gene regulatory program at the G_1/S-phase transition in pluripotent cells. Expedited expression of histone genes is mediated by a unique chromatin architecture reflected by major nuclease hypersensitive sites, atypical distribution of epigenetic histone marks, and a region devoid of histone octamers. We observed remarkable differences in chromatin structure—hypersensitivity and histone protein modifications—between human embryonic stem (hES) and normal diploid cells. Cell cycle-dependent transcription factor binding permits dynamic three-dimensional interactions between transcript initiating and processing factors at 5′ and 3′ regions of the gene. Thus, progression through the abbreviated G_1 phase involves cell cycle stage-specific chromatin-remodeling events and rapid assembly of subnuclear microenvironments that activate histone gene transcription to promote nucleosomal packaging of newly replicated DNA during stem cell renewal.

Human embryonic stem (hES) and induced pluripotent stem (iPS) cells maintain an undifferentiated state, are competent to proliferate indefinitely, and possess the ability to differentiate to all three germ layers (25, 33, 42, 45, 51, 52, 54, 60). The unique ability to self-renew and to give rise to any cell type of an organism reflects the therapeutic potential of pluripotent stem cells in regenerative medicine. Human ES and iPS cells have an abbreviated G_1 phase and lack a classical restriction (R) point that normally controls commitment for progression into S phase (3, 4, 23, 24). In contrast, proliferation of somatic cells is linked to growth factor-dependent passage through the R point in G_1 phase (43, 44). The precise mechanisms by which cell cycle kinetics are modulated as cells switch between pluripotent and phenotype-committed states are complex and remain to be established. Key cell cycle-related gene-activating events that occur between mitosis and S phase must be accelerated in the pluripotent state relative to those in phenotype-committed cells. More importantly, the absence of an R point in pluripotent cells necessitates reliance on other G_1/S-phase-related gene-regulatory mechanisms to control entry into S phase. To understand molecular events at the G_1/S-phase transition in pluripotent embryonic stem cells, it is necessary to identify genes that can be mechanistically examined for chromatin remodeling that accompanies gene activation.

There are fundamental architectural modifications in genome configurations during the abbreviated self-renewal cell cycle of pluripotent hES cells to establish competency for DNA replication. As hES cells exit mitosis during self-renewal, chromosome decondensation and immediate assembly of chromatin-related nuclear microenvironments essential for gene expression (e.g., histone locus bodies, or HLBs) are expedited (23). Another accelerated principal chromatin-remodeling event in hES cells is linked to the induction of DNA replication and concomitant packaging of newly replicated DNA into chromatin by histone octamers (i.e., composed of two heterodimers of the core histone proteins H4-H3 and H2A-H2B). Chromatin-related mechanisms control gene activation necessary for S-phase entry by rendering promoters selectively and rapidly accessible to regulatory factors. These events in the abbreviated G_1 phase of hES cells are temporally interposed between dynamic chromatin-remodeling events at the M/G_1 and G_1/S transitions.

Maintenance of an open chromatin structure is essential for the pluripotent state. For example, depletion of the chromatin-remodeling factor gene *Chd1* in mouse ES cells results in accumulation of heterochromatin and loss of pluripotency (20). The transcription factors Oct4, Sox2, and Nanog constitute the core regulatory circuitry of embryonic stem cells and sustain pluripotency by activating a great number of genes (10, 11, 34, 50). These pluripotency factors also repress cell lineage-specific regulators to maintain the undifferentiated state (5, 8, 9, 29, 31, 46). To retain options for differentiation into all cell types, the chromatin of undifferentiated ES cells is transcriptionally permissive, with pronounced sensitivity to nucleases and limited heterochromatinization, as well as highly dynamic binding of structural proteins (e.g., histones H2A and H2B, HP1), general transcription factors (e.g., GTF2a1, GTF2b), and chromatin-remodeling factors (e.g., Smarca4, Chd1) (16, 35). Upon differentiation of ES cells, chro-

Received 31 May 2012 Returned for modification 28 June 2012
Accepted 17 July 2012
Published ahead of print 23 July 2012
Address correspondence to Gary S. Stein, gary.stein@uvm.edu.
* Present address: Gary S. Stein, Department of Biochemistry, University of Vermont, Burlington, Vermont, USA; Janet L. Stein, Department of Biochemistry, University of Vermont, Burlington, Vermont, USA.

doi:10.1128/MCB.00736-12

matin structure becomes more compact and repressive (1, 16, 49). In contrast to the gene-selective chromatin remodeling that occurs during the cell cycle on a "mixed background" of euchromatin and heterochromatin in committed cells, active G_1 phase-related changes in chromatin architecture in ES cells must be achieved on a predominantly euchromatin background. Thus, identifying representative genes that are upregulated at the onset of S phase and remodeled in an open chromatin configuration is a significant priority.

The very short G_1 phase of ES cells is expected to temporally compress chromatin remodeling of genes that are transcriptionally induced at the G_1/S-phase transition. Therefore, it is important to establish how chromatin structure is locally reorganized to support activation of genomic loci that are essential for S-phase progression, while cells decondense chromatin following mitotic division in anticipation of accelerated S-phase entry. Equally important, pluripotent cells must rely on R-point-independent gene-regulatory mechanisms to achieve competence for S-phase entry. Thus, it is necessary to characterize genes that are induced at the G_1/S-phase transition to understand how pluripotent cells commit to chromatin duplication. Significantly, we find that activation of genes encoding histones—the very proteins that package DNA as chromatin and convey epigenetic regulatory information—is the most prominent gene regulatory program at the onset of S phase in human ES cells. This induction is mediated by active remodeling of chromatin, dynamic recruitment of gene regulatory factors, and epigenetic marking of nucleosomes that are distinctly organized at human histone loci. These findings establish a histone gene-selective reconfiguration of chromatin architecture that proceeds in parallel with decondensation of chromatin as cells exit from mitosis through an abbreviated G_1 phase in preparation for S phase in pluripotent human ES cells.

MATERIALS AND METHODS

Cell culture. Human embryonic stem cell line H9 (WA09; WiCell Research Institute, Madison, WI) and human iPS cell lines A6 and D1 (25) were maintained under nondifferentiated conditions in hESC medium (Dulbecco modified Eagle medium–nutrient mixture F-12, 20% KnockOut serum replacement, 1 mM L-glutamine, 1% nonessential amino acids, 0.1 mM β-mercaptoethanol [all from Gibco/Invitrogen, Carlsbad, CA], 4 ng/ml β-fibroblast growth factor [β-FGF] [R & D Systems, Minneapolis, MN]) at 37°C with 5% CO_2 in a humidified incubator. Cells were routinely examined for stem cell markers and normal karyotype. Pluripotent cells were maintained on inactivated mouse embryonic fibroblast-coated plates prepared as described before (3). Normal diploid TIG-1 fibroblasts were cultured in Nunclon Δ surface dishes (Nunc, Rochester, NY) and maintained in MEM–10% fetal bovine serum (FBS), 2 mM L-glutamine, 100 U/ml penicillin, and 100 μg/ml streptomycin (all from Gibco/Invitrogen) at 37°C and 5% CO_2 in a humidified incubator. Normal diploid IMR-90 fibroblasts were maintained in BME (Gibco/Invitrogen), 10% FBS (Atlanta Biologicals), 2 mM L-glutamine, 100 U/ml penicillin, and 100 μg/ml streptomycin (both from Gibco/Invitrogen) at 37°C and 5% CO_2 in a humidified incubator. Normal diploid WI-38 fibroblasts were maintained in MEM-EBSS (Gibco/Invitrogen), 10% FBS (HyClone), 2 mM L-glutamine, 1 mM sodium pyruvate, 0.1 mM nonessential amino acids, 100 U/ml penicillin, and 100 μg/ml streptomycin (all from Gibco/Invitrogen) at 37°C and 5% CO_2 in a humidified incubator. Human ES cells (H9) and TIG-1 fibroblasts were synchronized using nocodazole (200 ng/ml and 50 ng/ml, respectively) for 16 h, and samples were taken at different time points after release. Normal WI-38 fibroblasts were synchronized by serum deprivation for 72 h, and samples were taken at different time points after release in the same medium containing 20% serum.

RNA isolation, cDNA synthesis, and real-time quantitative PCR. Total RNA was either prepared using TRIzol reagent (Invitrogen) followed by DNase I treatment (DNA-free RNA kit; Zymo Research, Irvine, CA) or column purified using the RNeasy Plus minikit or the miRNeasy minikit (Qiagen, Valencia, CA). Synthesis of cDNA was performed with the SuperScript first-strand synthesis system III (Invitrogen). The relative transcript level was determined by the $\Delta\Delta C_T$ method using the cycle threshold (C_T) obtained in the 7300 sequence detection system (Applied Biosystems, Foster City, CA) and iTaq SYBR green supermix with ROX (Bio-Rad Laboratories, Hercules, CA). The following primer pairs were used for human transcripts: for *HIST2H4* (histone H4/n), AGC TGT CTA TCG GGC TCC AG (forward) and CCT TTG CCT AAG CCT TTT CC (reverse); for *HIST1H3I* (histone H3/f), ATG GCA CGA ACA AAG CAA AC (forward) and GTA GCG GTG GGG CTT CTT (reverse); for *CCNE2* (cyclin E2), CCG AAG AGC ACT GAA AAA CC (forward) and GAA TTG GCT AGG GCA ATC AA (reverse); for *CCNB2* (cyclin B2), ACT GCT CTG CTC TTG GCT TC (forward) and TTT CTC GGA TTT GGG AAC TG (reverse).

Gene arrays. GeneChip human gene 1.0 ST arrays (Affymetrix, Santa Clara, CA) were used to analyze total RNA isolated from hES cells and normal human fibroblasts (TIG-1). These arrays interrogate 28,869 well-annotated genes with 764,885 distinct probes and offer whole-transcript coverage with multiple probes distributed across the full length of the gene. DNA-free total RNA samples from synchronized hES cells in G_1 or S phase (1.5 or 4 h after release from a nocodazole [Sigma, St. Louis, MO] block) were labeled and analyzed according to the manufacturer's instructions at the Genomics Core Facility at University of Massachusetts Medical School. Fold ratios (R values) were determined to assess the relative expression of genes in G_1 versus S phase.

Sensitivity to nucleases. Nuclease hypersensitivity was assessed by digestion of human embryonic stem (hES) or normal diploid fibroblasts (TIG-1 or IMR-90) nuclei with DNase I. Nuclei were isolated by Dounce homogenization of cells in 10 ml of RSB buffer (10 mM Tris-HCl, pH 7.4, 10 mM NaCl, 5 mM $MgCl_2$) supplemented with 0.5% Nonidet P-40. Nuclei were recovered by centrifugation at 1,000 × *g* for 5 min at 4°C. Nuclei were washed twice with RSB buffer and recovered by centrifugation as described before. Nuclei were then resuspended in RSB buffer supplemented with 1 mM $CaCl_2$ and incubated with increasing concentrations of DNase I (DPRF; Worthington Biochemical Corporation, Lakewood, NJ) for 10 min at room temperature with gentle agitation. Reactions were stopped by the addition of 150 μl of stop buffer (50 mM EDTA and 0.5% SDS). DNA was purified by standard phenol-chloroform-isoamyl alcohol extraction and completely digested with PstI/BamHI (New England BioLabs, Ipswich, MA), electrophoresed in an 2% agarose gel in 1× TAE buffer (40 mM Tris-acetate, 1 mM EDTA, pH 8.0), and transferred to Hybond-N+ membranes (GE Healthcare, Piscataway, NJ) according to the manufacturer's instructions. Southern blotting was performed using a probe prepared by digesting a plasmid carrying the *HIST2H4* (histone H4/n) gene with XbaI/PstI and labeling using random primers (Invitrogen) spanning the region between nucleotides −1,048 and +1,264 (probe, +831/+1,264; see Fig. 2A) relative to the transcriptional start site (TSS).

ChIP assays. For standard chromatin immunoprecipitation (ChIP) assays, human ES cells and normal WI-38 fibroblasts were cross-linked at room temperature in ESC medium or incomplete WI-38 medium with formaldehyde for 10 min and 6 min, respectively. To increase the likelihood of detecting occupancy of non-DNA binding proteins, we performed dual cross-linking using two long-arm protein-protein cross-linking agents: ethylene glycol-bis(succinimidyl succinate) (EGS) and dimethyl 3,3′-dithiobispropionimidate · 2HCl (DTBP) (Thermo Scientific, Rockford, IL). Human ES cells were separately incubated with EGS or DTBP in hESC medium for 20 min at room temperature before the addition of formaldehyde. Cross-linking was stopped by the addition of

glycine for 5 min at room temperature. Cells were harvested in ice-cold PBS containing 1× complete protease inhibitor (Roche Applied Science, Indianapolis, IN), 1× phosphatase inhibitor cocktail I (Calbiochem, Gibbstown, NJ), 1× phosphatase inhibitor cocktail II (Calbiochem), and 20 mM sodium butyrate (Sigma). Cells were rapidly frozen in liquid nitrogen and stored at −80°C until use. Cell pellets were resuspended in buffer 1 (50 mM HEPES-KOH, pH 7.5, 140 mM NaCl, 1 mM EDTA, 10% glycerol, 0.5% Nonidet P-40, 0.25% Triton X-100, 1× protease inhibitors), and after centrifugation the pellet was resuspended in buffer 2 (10 mM Tris-HCl, pH 8.0, 200 mM NaCl, 1 mM EDTA, 0.5 mM EGTA, 1× protease inhibitors). The pelleted nuclei were then resuspended in buffer 3 (10 mM Tris-HCl, pH 8.0, 100 mM NaCl, 1 mM EDTA, 0.5 mM EGTA, 0.1% sodium deoxycholate, 0.5% *N*-lauroylsarcosine, 1× protease inhibitors) and sonicated with a Misonix ultrasonic liquid processor S-4000 (QSonica, LLC, Newtown, CT). Chromatin was recovered from the supernatant, and the efficiency of sonication was analyzed by electrophoresis on an agarose gel to monitor the size of sheared DNA (between 250 and 650 bp). Chromatin was aliquoted, rapidly frozen in liquid nitrogen, and stored at −80°C until use. ChIP assays were initiated by diluting chromatin either in buffer FA (50 mM HEPES-KOH, pH 7.5, 140 mM NaCl, 1 mM EDTA, 1% Triton X-100, 0.1% sodium deoxycholate, 0.1% SDS, 1× protease inhibitors) for H3K4me3 (Abcam, Cambridge, MA) antibody or in sonication buffer 3 for the remaining antibodies. The following antibodies were used per 100 μg chromatin: HINFP (5 μl of 802K rabbit polyclonal antiserum) (40), RNA polymerase II (pol II) (2.5 μl of 8WG16 mouse monoclonal IgG2a, ascites fluid; catalog no. MMS-126R; Covance [Princeton, NJ]), $p220^{NPAT}$ (5 μl of rabbit polyclonal serum kindly provided by J. Wade Harper, Harvard Medical School [32], or 5 μg of mouse monoclonal IgG2b; catalog no. 611344; BD Biosciences [San Jose, CA]), LSM10 (2 μg of mouse monoclonal IgG2a; catalog no. BMR00504; Bio Matrix Research Inc. [Nagareyama City, Chiba, Japan]), LSM11 (10 μl of rabbit affinity-purified antibody [47]), FLASH (12 μl of rabbit affinity-purified antibody [7]), SLBP (10 μl of rabbit polyclonal antibody [17]), CPSF73 (1 μg of rabbit affinity-purified antibody; catalog no. A301-091A; Bethyl Laboratories, Inc. [Montgomery, TX]), histone H3 (5 μg of rabbit polyclonal IgG; catalog no. ab1791; Abcam), H3K4me3 (5 μl of rabbit polyclonal serum; catalog no. 39159; Active Motif [Carlsbad, CA], or 20 μg of mouse monoclonal IgG2b; catalog no. ab1012; Abcam), H3K9ac (5 μg of rabbit polyclonal IgG; catalog no. ab4441; Abcam), H3K27me3 (5 μg of rabbit polyclonal IgG; catalog no. 07-449; Millipore [Billerica, MA]), H4K12ac (5 μl of rabbit polyclonal serum; catalog no. 07-595; Millipore), and H4K16ac (5 μg of rabbit polyclonal serum; catalog no. 07-329; Millipore). After incubation with the antibodies overnight at 4°C, chromatin-antibody complexes were recovered by incubating with preblocked protein A/G-agarose beads (Santa Cruz Biotechnology, Santa Cruz, CA) for 2 h at 4°C on a rotating wheel. Beads were washed, DNA was eluted, and cross-links were reversed. DNA was recovered by ethanol precipitation and analyzed by quantitative PCR (qPCR). ChIP results were expressed as percent input. Alternatively, DNA concentration was quantified by fluorometry (Qubit, Invitrogen), and all samples were adjusted to the same concentration. DNA (0.5 ng) was analyzed by qPCR and expressed as fold enrichment ($2^{-[\text{ChIP } CT - \text{input } CT]}$). The following primer pairs were used for H4: primer 1 (−648 to −519) (forward, ACG TCC ATG AGA AAG CTT GG; reverse, CAG GTT CGC CAT AAT TCC TG); primer 2 (−412 to −323) (forward, ATA AGC ACG GCT CTG AAT CC; reverse, ATA AGC ACG GCT CTG AAT CC); primer 3 (−152 to −73) (forward, ATA AGC ACG GCT CTG AAT CC; reverse, ATA AGC ACG GCT CTG AAT CC); primer 4 (+4 to +69) (forward, ATA AGC ACG GCT CTG AAT CC; reverse, CCT TTG CCT AAG CCT TTT CC); primer 5 (+50 to +177) (forward, CCT TTG CCT AAG CCT TTT CC; reverse, CCT TTG CCT AAG CCT TTT CC); primer 6 (+276 to +369) (forward, CCT TTG CCT AAG CCT TTT CC; reverse, CCT TTG CCT AAG CCT TTT CC); primer 7 (+348 to +473) (forward, CCT TTG CCT AAG CCT TTT CC; reverse, CCT TTG CCT AAG CCT TTT CC); primer 8 (+916 to +1032) (forward, CCT TTG CCT AAG CCT TTT CC; reverse, CCT TTG CCT AAG CCT TTT CC). The following primer pairs were used for H3: primer 1 (−678 to −559) (forward, AAG TGC CGG CTT CTC TGA TA; reverse, CGC ATT GGT AGC GGT AAA GT); primer 2 (−430 to −251) (forward, CGC ATT GGT AGC GGT AAA GT; reverse, CGC ATT GGT AGC GGT AAA GT); primer 3 (−71 to +37) (forward, CGC ATT GGT AGC GGT AAA GT; reverse, ACT TGC GAG CTG TTT GCT TT); primer 4 (+4 to +78) (forward, ACT TGC GAG CTG TTT GCT TT; reverse, ACT TGC GAG CTG TTT GCT TT); primer 5 (+173 to +245) (forward, ACT TGC GAG CTG TTT GCT TT; reverse, ACT TGC GAG CTG TTT GCT TT); primer 6 (+349 to +455) (forward, GCC AAA CGC GTC ACT ATT ATG; reverse, GCC AAA CGC GTC ACT ATT ATG); primer 7 (+429 to +605) (forward, GCC AAA CGC GTC ACT ATT ATG; reverse, GCC AAA CGC GTC ACT ATT ATG); primer 8 (+1037 to +1210) (forward, GCC AAA CGC GTC ACT ATT ATG; reverse, GCC AAA CGC GTC ACT ATT ATG).

Immunofluorescence microscopy. Human ES H9 cells were grown on coverslips, and immunofluorescence microscopy analysis was carried out as described previously (21–23). Briefly, cells were fixed with 3.7% formaldehyde for 10 min, permeabilized with 0.25% Triton X-100 for 20 min, and then treated with primary antibody for 1 h at 37°C, followed by detection using the appropriate fluorescence-tagged secondary antibody. The nuclei were counterstained with DAPI (4′,6-diamidino-2-phenylindole). Cells were viewed under an epifluorescence Zeiss Axioplan 2 microscope, and images were captured using a Hamamatsu (C4742-95) charge-coupled-device (CCD) camera and analyzed by Metamorph imaging software (Universal Imaging, West Chester, PA). The following antibodies were used: monoclonal $p220^{NPAT}$ (mouse monoclonal, 1:1,000; BD Biosciences, San Jose, CA), polyclonal $p220^{NPAT}$ (rabbit polyclonal, 1:1,000), polyclonal-T1270-$p220^{NPAT}$ (rabbit polyclonal, 1:500) (32, 61), LSM11 (rabbit polyclonal, 1:500) (47), and RNA pol II (mouse monoclonal clone 8WG16, 1:1,000; Covance, Princeton, NJ). Secondary antibodies conjugated with Alexa Fluor dyes were all used at 1:800.

Proximity ligation assay. The proximity ligation assay protocol was derived from the previously published chromosome conformation capture (3C) method (39) with modifications. Briefly, 4.6 million hES H9 cells were cross-linked and treated as described for ChIP assays. Nuclei were digested with FatI (R0650, New England BioLabs) for 2 h at 55°C and then overnight at 42°C. To reduce the background ligation frequency, the ligation step was carried out in >80 separate reactions in which each reaction mixture contained 0.5 genomic copy of DNA. Cross-links were reversed, and DNA was purified by phenol-chloroform extraction followed by ethanol precipitation. To control for primer efficiency and to serve as a random ligation control, a bacterial artificial chromosome (BAC) (RP11-1118G19; BACPAC) spanning the histone *HIST2H4* region was used. The BAC template was prepared in the same fashion as the hES cell template but without the cross-link step. The results of the assays represent data obtained from two different sets of ligation reactions where two different PCRs were performed in triplicate for each data point for each sample. The PCR products were separated in a 1% agarose gel and quantified by the Gel-Quant software (www.gelquant.org). The following primer pairs were used: FatI_H4_1_FW, GGA GAA CTG TTT TGT TTC TTC CA; FatI_H4_1_RV, GGA CCG AGC CAC TGT ATT TTA G; FatI_H4_2_FW, TCA ATC TGG TCC GAT ACT CTT GT; FatI_H4_2_RV, CCT GAA TGT TGT CTC TCA AGA CC; FatI_H4_3_FW, AAG GTG TTC CTG GAG AAT GTG AT; FatI_H4_3_RV, ACT CCT CAG ATG AGC AAG TGG T; FatI_H4_4_FW, TTG CTC TTC TGG TGC AGT ATA GG; FatI_H4_4_RV, AAT GAA AAC CTA AGG CTG CTT CT; FatI_GDR2_1FW, TGA CCT CCA GAA TGG TAA GAG AA; FatI_GDR2_2RV, TTG TCT AGG AGA GCT CAG TCC AC. Statistical analyses of differences in ligation frequencies between the *HIST2H4* gene and a gene desert region (GDR) were evaluated using general linear mixed models (36). Models were fit by restricted maximum likelihood estimation (12) using the SAS Proc Mixed procedure (48). In the presence of significant differences among means, pairwise comparisons were made using Tukey's honestly significant difference (HSD) multiple-comparison

A

Genes \ Fold	Human ES cells (H9) ↑ (>1.2)	Human ES cells (H9) ↓ (<0.83)	Human Fibroblasts (TIG-1) ↑ (>1.2)	Human Fibroblasts (TIG-1) ↓ (<0.67)
Total	107	53	135	584
Histone	40 (37%)*	0	22 (16%)**	1
Non-histone	67 (63%)	53	113 (84%)	583

* 61% of total replication-dependent histone genes
** 33% of total replication-dependent histone genes

B

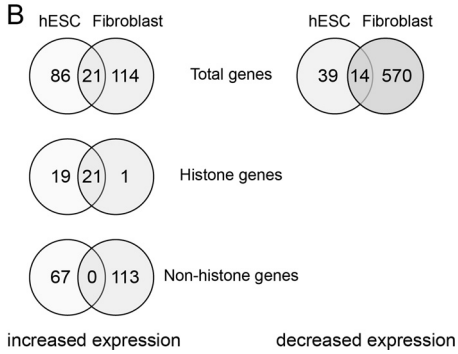

FIG 1 Gene expression profiling during the G_1/S-phase cell cycle transition. (A) Comparative microarray analysis of genes exhibiting >1.2-fold differences in expression in human embryonic stem (hES) cells or normal human fibroblasts (TIG-1). Expression profiling was performed using GeneChip human gene 1.0 ST arrays from Affymetrix. (B) Venn diagrams showing the numbers of genes with increased and decreased expression during the G_1/S-phase transition in hES versus TIG-1 cells.

procedure (55) utilizing the estimated covariance matrix to account for correlated observations. The distributional characteristics of outcome measures were evaluated by applying the Kolmogorov-Smirnov goodness-of-fit test for normality (13) to residuals from fitted linear models and by inspection of frequency histograms of these residuals. In some cases, natural logarithms of outcomes were applied to better approximate normally distributed residuals. All computations were performed using the SAS version 9.1.3 (SAS Institute, 2006) and SPSS version 14 (SPSS, Inc., 2005) statistical software packages. Statistical significance is defined as present when associated *P* values are less than 0.05.

RESULTS

Histone gene expression is the most prominent genomic program upregulated at the G_1/S-phase transition in human embryonic stem cells. Gene activation during the human embryonic stem (hES) cell cycle requires gene-selective chromatin remodeling. To identify model genes for mechanistic studies, we applied an unbiased strategy to characterize which genes are maximally upregulated at S-phase entry in hES cells. Gene expression profiling reveals that 107 genes are elevated as synchronized hES H9 cells traverse from G_1 to S phase. A substantial subset of these genes, preferentially expressed in S phase, encode DNA replication-dependent histone proteins ($n = 40$), including linker histone H1 ($n = 4$) and 36 core histones (H2A, 13; H2B, 9; H3, 7; H4, 7), corresponding to 61% of the full complement of human histone genes that are modulated by >1.3-fold (Fig. 1A). Because histones are required for packaging newly replicated DNA as chromatin, this finding is consistent with biological expectations.

Many histone genes are upregulated by 2-fold or more in S phase (e.g., *HIST1H3B* and *HIST1H2BM*), and their expression is roughly proportional to the total number of gene copies for each subtype. Expression of only 17 genes is increased on average by 2-fold or more, and 15 of these are histone genes. As anticipated, none of the DNA replication-independent histone gene variants exhibits significant S-phase-related changes in mRNA levels (e.g., *H1FX*). Only two nonhistone genes are increased by 2-fold or more in hES cells: *MDM2* (2.1-fold), which encodes a protein that antagonizes the growth suppression function of p53 (6, 18, 19, 30), and a pseudogene (ENST00000354652) of unknown relevance. We also detected 65 other nonhistone genes that showed elevated expression, but none of these were modulated by more than 2-fold in hES cells. As expected, no histone genes were found to have decreased expression in S phase compared to G_1 phase in hES cells (53 nonhistone genes were found to have decreased expression). For comparison, in normal human fibroblasts there are only 22 histone genes and as many as 113 nonhistone genes that exhibit elevated expression (Fig. 1A and B). These results demonstrate that histone genes are the most prominently modulated genes during the G_1/S-phase transition in human embryonic stem cells.

Histone gene expression in pluripotent cells is supported by nuclease hypersensitivity and association of the transcription factor HINFP and RNA polymerase II with histone H4 loci. Because histone gene expression is the most prominent gene regulatory event during the transition from G_1 to S phase in hES cells, we defined the transcriptional mechanisms that control a representative histone H4 gene (*HIST2H4* or H4/n gene). Analysis of nuclease sensitivity (56) of the genomic histone *HIST2H4* locus to DNase I reveals changes in chromatin structure that accompany increased histone gene expression in hES cells. There are striking hypersensitive sites (HSS) at the promoter (nucleotide [nt] −130), transcriptional start site (nt +1), coding region (nt +290), and beyond the 3′ end of the histone H4 gene (nt +490) (Fig. 2A). Normal human TIG-1 and IMR-90 fibroblasts show HSS at the same location (Fig. 2A), but they are significantly more resistant to DNase I digestion, even at higher nuclease concentrations (Fig. 2A). Thus, in hES cells the entire histone H4 gene locus, including its 5′ and 3′ flanking regions, is in a more open and highly accessible chromatin conformation.

Enhanced histone H4 gene expression in pluripotent hES cells is mediated by association of the histone H4 gene-specific transcription factor HINFP and RNA polymerase II with the histone *HIST2H4* gene. Chromatin immunoprecipitation (ChIP) analysis shows that HINFP and RNA pol II are both present at the histone H4 gene in hES cells (Fig. 2B). HINFP binds distal to RNA pol II in the histone H4 gene promoter: maximal HINFP binding is centered at its cognate element (site II) in the proximal promoter, while RNA pol II is associated with the transcriptional start site (TSS), as well as with downstream sequences. ChIP results with two distinct induced pluripotent stem (iPS) cell lines (iPS A6 and iPS D1) (25) and a normal human lung fibroblast cell line (WI-38) show that both HINFP and RNA pol II tandemly associate with the histone H4 gene promoter as in hES H9 cells (Fig. 3A). The relative association of RNA pol II and HINFP in WI-38 is less pronounced, consistent with the smaller fraction of WI-38 cells progressing through S phase. Therefore, HINFP and RNA pol II association with the histone H4 gene is a general property of proliferating cells in the pluripotent state.

The HINFP motif in site II is located directly upstream (~10 bp, or one DNA helix turn) of the TATA box, which suggests a molecular mechanism by which HINFP together with the protein

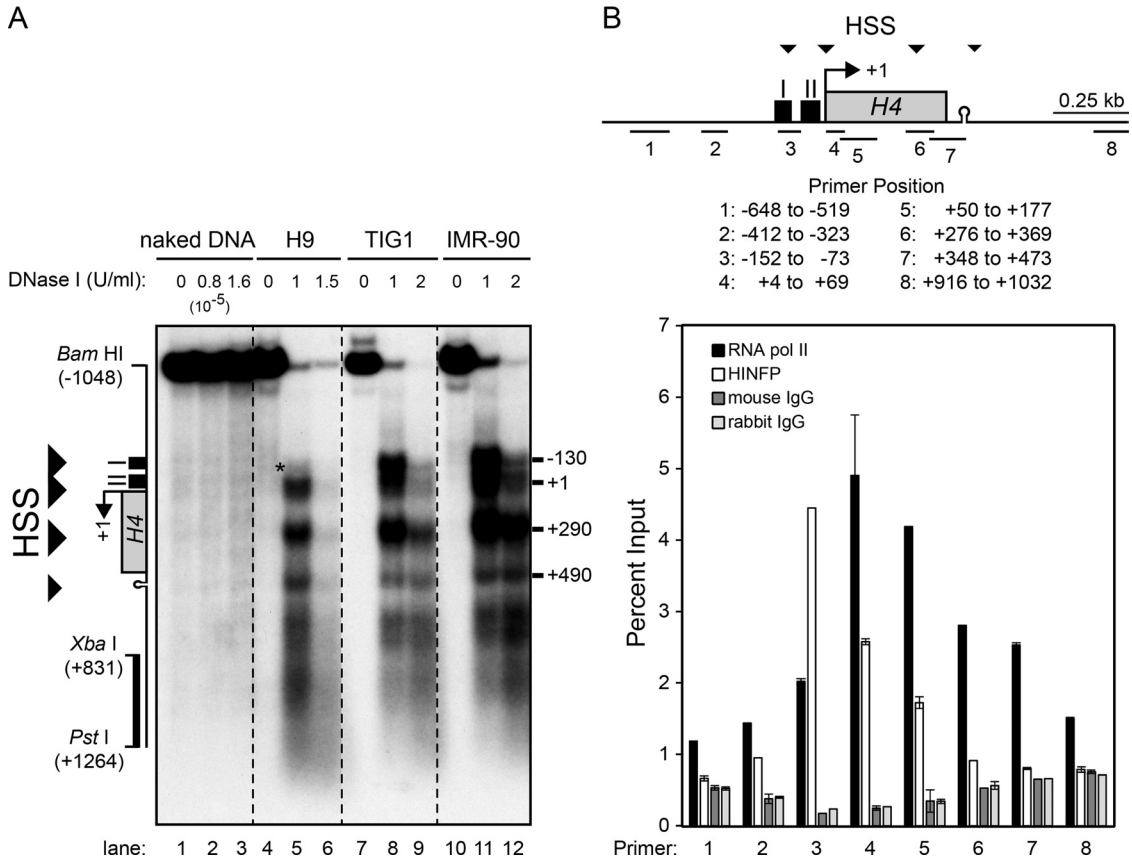

FIG 2 Chromatin architecture of the human histone H4 gene in hES cells. (A) DNase I hypersensitivity at the human histone H4 gene (*HIST2H4*). Nuclei were isolated from hES cells (lanes 4 to 6) and normal diploid fibroblasts (TIG-1 and IMR-90; lanes 7 to 9 and 10 to 12, respectively), and DNA was prepared as described in Materials and Methods. Naked genomic DNA from hES cells digested with increasing amounts of DNase I was used as a control (lanes 1 to 3). The positions of the DNase I hypersensitive sites (HSSs) are shown on the right. A schematic representation of the human histone H4 gene, restriction sites, transcription start site, probe used in Southern blots, and HSSs (arrowheads) is shown on the left. Human ES cells show increased nuclease sensitivity at lower DNase I concentrations than normal diploid fibroblasts (compare lane 6 with lanes 9 and 12); the asterisk (nt −130, lane 5) designates an HSS in hES cells that is observed only at short digestion times. (B) Chromatin landscape of the histone H4 gene in human pluripotent cells. The top panel shows a schematic of the genomic organization of the human histone H4 gene. Transcriptional binding sites I and II, the set of primers (lines 1 to 8) used for analyses and their location, the HSSs (arrowheads), and the sequence representing the typical stem-loop structure found in histone mRNAs are shown. The bottom panel shows chromatin immunoprecipitation analysis for RNA pol II and HINFP at the human histone H4 gene in human embryonic stem cells.

complex of general transcription factors interacting with the TATA box may mediate RNA polymerase II recruitment. Importantly, our data show that strong interactions of HINFP and RNA pol II occur within the region of the histone H4 locus that is maximally accessible to DNase I, reflecting a highly open chromatin structure at the TSS. To test whether HINFP and RNA pol II cooccupancy is observed for other histone genes or is limited to HINFP-dependent histone H4 genes, we assessed RNA pol II binding to a HINFP-independent histone H3 gene (*HIST1H3I* or H3/f gene). ChIP analysis shows that RNA pol II is present at the TSS of the histone H3 gene in hES cells but that HINFP binding is negligible (Fig. 3D). Our data suggest that binding of RNA pol II to histone gene promoters in hES cells is characteristic of expressed histone genes. However, HINFP supports the positioning of RNA pol II only near the TSS of histone H4 and not H3 genes. Binding of RNA pol II to other histone genes may be mediated by other histone gene-specific transcription factors.

Active epigenetic histone modifications mark dynamically transcribed histone genes in pluripotent cells. The epigenetic landscape of chromatin at the histone genes in human pluripotent cells is reflected by distinct covalent modifications of histone proteins related to transcriptional activation. We performed ChIP analysis for trimethylation of histone H3 lysine 4 (H3K4me3) and acetylation of histone H3 lysine 9 (H3K9ac) as representative active marks, while trimethylation of histone H3 lysine 27 (H3K27me3) was monitored as a repressive mark. In all three pluripotent stem cells (hES H9, iPS A6, and iPS D1) we detected high levels of H3K4me3 and H3K9ac both upstream and downstream of the TSS (Fig. 3B) of the histone H4 gene. In each case, we observed decreased levels of these marks at the TSS. This finding is indicative of a nucleosome-free region at the TSS, consistent with previous observations in human cancer cell lines (27, 41). Similar results were obtained for the histone H3 gene (Fig. 3E). In contrast, the repressive mark H3K27me3 was found to be minimally present at both H4 and H3 loci in all three pluripotent stem cells and hES cells, respectively, as expected from an actively transcribed gene contained within an open chromatin context (Fig. 3C and F). We note

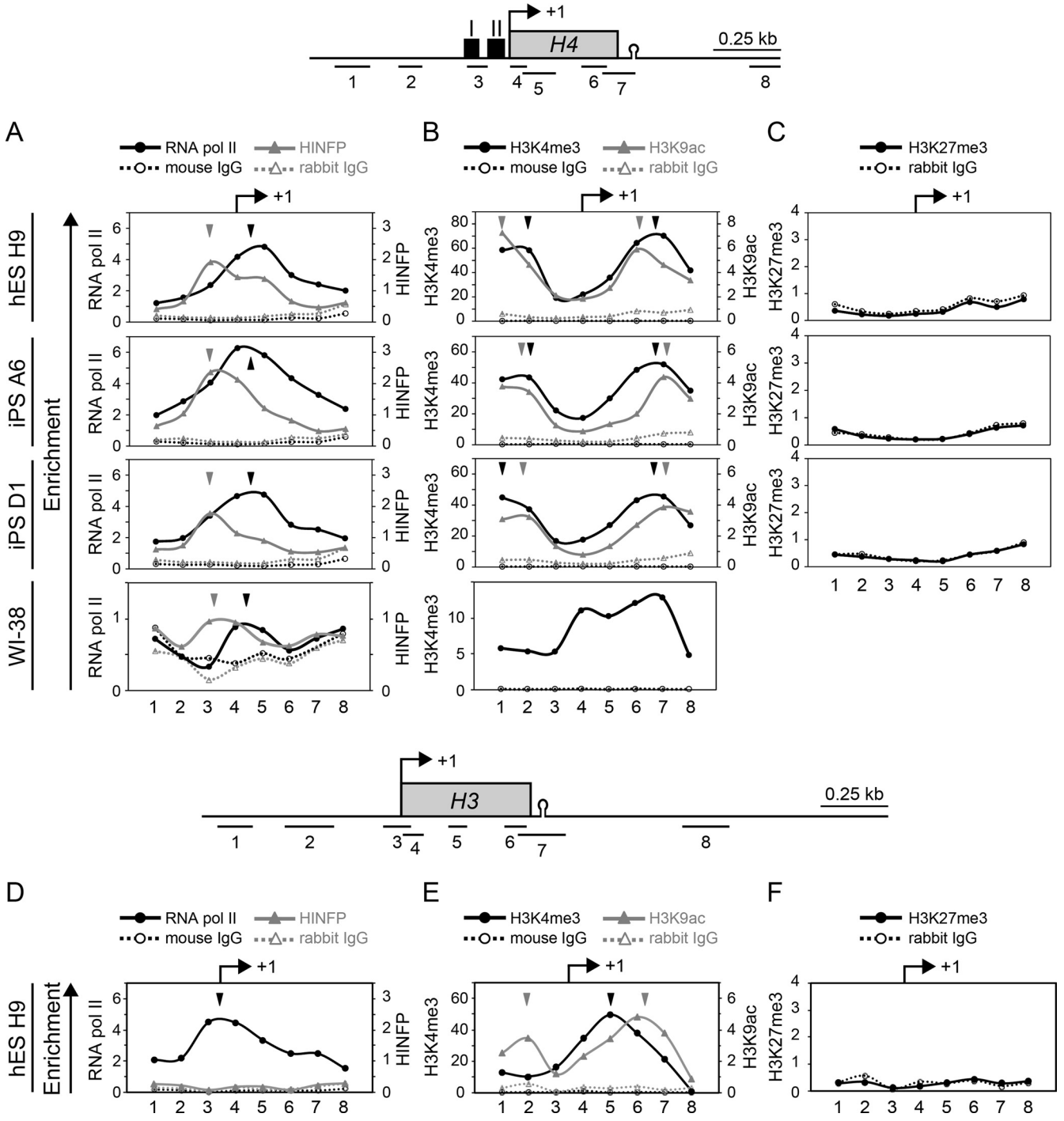

FIG 3 Active chromatin marks at the human histone H4 and H3 gene loci in human pluripotent and normal diploid cells. (A) Interaction of RNA pol II and HINFP with the human histone H4 gene (*HIST2H4*) in human pluripotent cells (hES H9, iPS A6, iPS D1) and normal fibroblasts (WI-38). The top panel shows a schematic of the genomic organization of the human histone H4 gene as described in Fig. 2. Maximal interaction of HINFP (gray arrowheads) with the histone H4 gene is distal to that of RNA pol II (black arrowheads) in all three pluripotent cells and in normal fibroblasts (WI-38). The values obtained for ChIP antibodies and control IgGs are represented, respectively, by continuous and dotted lines. (B) Chromatin immunoprecipitation analysis of epigenetic marks of the histone H4 gene in human pluripotent cells and normal fibroblasts (WI-38). Solid lines represent the epigenetic marks H3K4me3 (black) and H3K9ac (gray), and dotted lines represent mouse or rabbit ChIP control IgGs for H3K4me3 (black) and H3K9ac (gray), respectively. (C) The human histone H4 gene lacks the epigenetic repressive mark H3K27me3 in all three pluripotent cell lines (hES H9, iPS A6, and iPS D1). Solid lines represent the epigenetic mark (black) and dotted lines represent rabbit ChIP control IgG (black) for H3K27me3. (D) Interactions of RNA pol II and HINFP with the human histone H3 gene (*HIST1H3I*) in hES H9 cells. The top panel shows a schematic of the genomic organization of the human histone H3 gene. The locations of primers (lines 1 to 8) used for ChIP analyses and the typical stem-loop structure found in histone mRNAs are shown. Values obtained for ChIP antibodies and control IgGs are represented, respectively, by continuous and dotted lines. (E) Chromatin immunoprecipitation analysis of epigenetic marks at the histone H3 gene in hES H9 cells. Solid lines represent the epigenetic marks H3K4me3 (black) and H3K9ac (gray), and dotted lines represent mouse or rabbit ChIP control IgGs for H3K4me3 (black) and H3K9ac (gray), respectively. (F) The human histone H3 gene lacks the epigenetic repressive mark H3K27me3 in hES cells. Solid lines represent the epigenetic mark (black) and dotted lines represent rabbit ChIP control IgG (black) for H3K27me3.

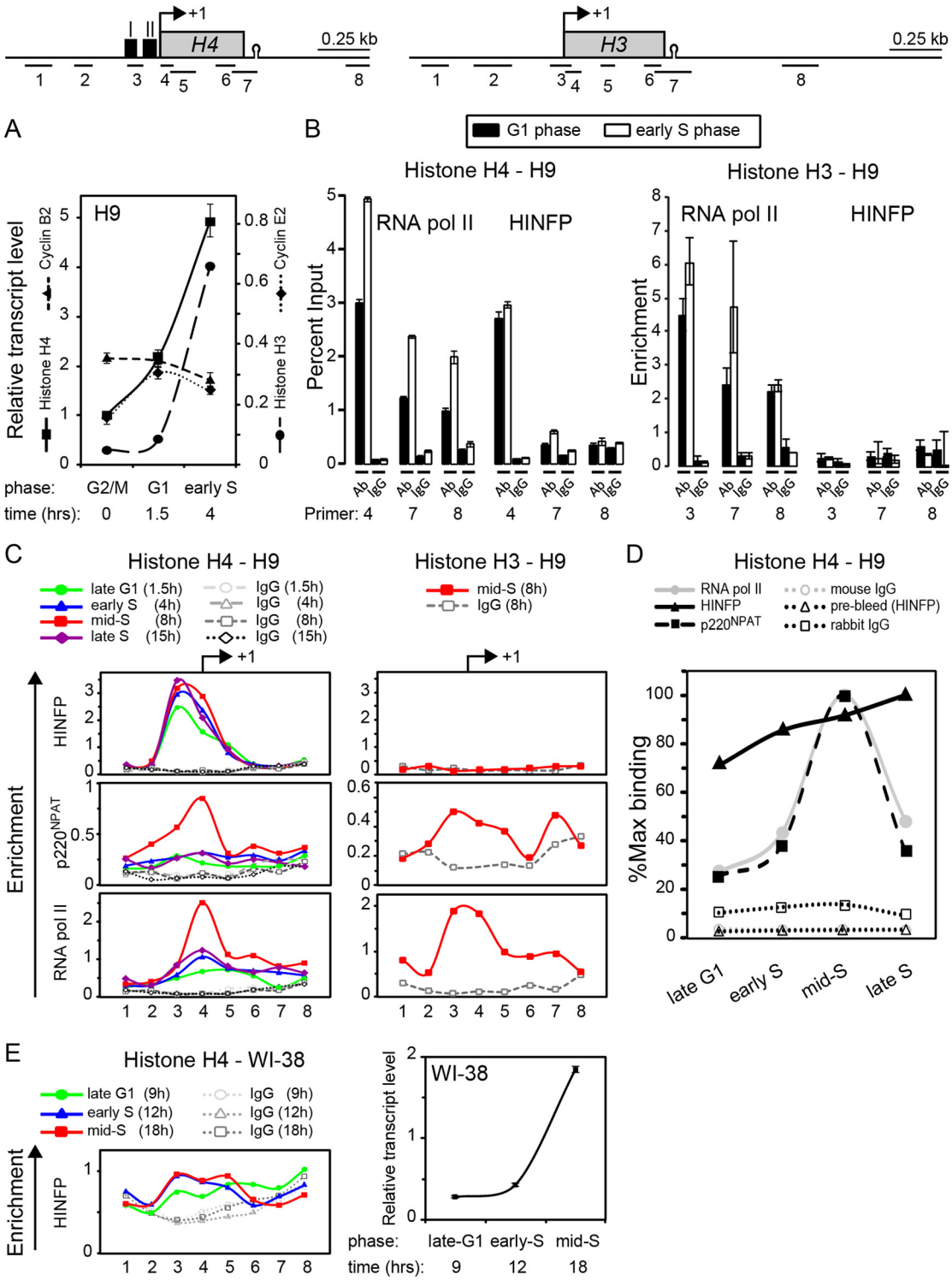

FIG 4 Selective occupancy of human histone genes during the pluripotent cell cycle. Human embryonic stem cells were synchronized in the G_2/M phase of the cell cycle by a nocodazole block and then released into the cell cycle. The top portion shows a schematic of ChIP primers relative to the genomic organization of the human histone H4 and H3 genes as described in Fig. 2. (A) Relative mRNA levels of cell cycle markers in synchronized hES H9 cells. An increase in the levels of histone H4 (solid line) and H3 (dashed line) RNAs and a decrease in cyclin E2 RNA (dotted line) confirm transition of cells from G_1 to early S phase. (B) Chromatin immunoprecipitation analysis of the human histone H4 (left panel) and H3 (right panel) genes in hES H9 cells at the G_1/S-phase boundary. (C) ChIP analysis of the histone H4 (left panel) and H3 (right panel) promoters during the cell cycle in hES H9 cells. Association of HINFP (top panels), the histone cofactor $p220^{NPAT}$ (middle panels), and RNA pol II (bottom panels) with the histone H4 and H3 genes is shown. (D) Temporal changes in binding of proteins at the site of maximal occupancy in the histone H4 locus during the hES cell cycle (around the TSS for RNA pol II and $p220^{NPAT}$ and around site II for HINFP). (E) ChIP analysis of HINFP association with the histone H4 gene during the cell cycle in normal fibroblasts (left panel). Human WI-38 cells were synchronized by serum deprivation and then released into the cell cycle by serum stimulation. Histone H4 transcript profile (right panel) confirms synchrony of WI-38 cells.

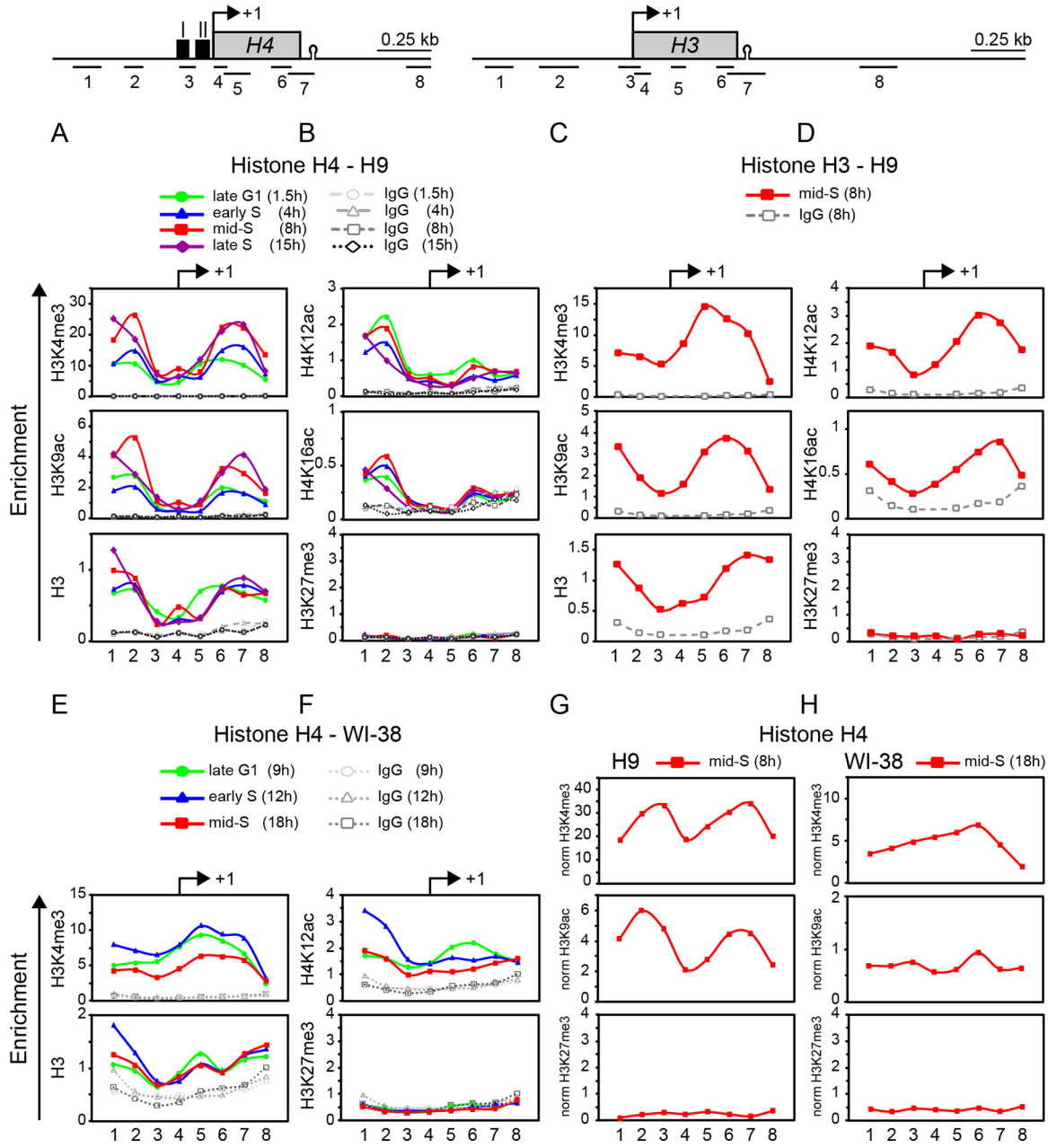

FIG 5 Epigenetic landscape of human histone genes. Chromatin immunoprecipitation analysis was performed with hES and WI-38 cells that were synchronized in the G_2/M phase by a nocodazole block and in G_0 by serum deprivation, respectively (details in Fig. 4 legend). Covalent modifications of histone proteins H3K4me3, H3K9ac, and total histone H3 (A and C) and H4K12ac, H4K16ac, and H3K27me3 (B and D) in hES cells at the human histone H4 and H3 genes are shown. Covalent modifications of histone proteins H3K4me3 and histone H3 (E) and H4K12ac and H3K27me3 (F) in WI-38 cells at the histone H4 locus are shown. Epigenetic marks normalized to total histone signal in hES cells (G) and fibroblasts (H) during the maximal occupancy of histone genes at mid-S phase are also shown. The top panels show the location of ChIP primers for histone H4 and H3 genes as described in Fig. 2.

that H3K27me3 was clearly detected at the *GATA6* and *OSX* loci that are not expressed in hES cells (data not shown). We also observed the presence of the active mark H3K4me3 in fibroblasts (Fig. 3B, bottom panel), although we note a striking difference in its association with the histone H4 locus compared with that of pluripotent cells: we detected high levels of H3K4me3 in the fibroblast cell line at the TSS, coding region, and 3′ end. These results indicate that the open chromatin structure of the histone gene loci in pluripotent cells exhibits transcriptionally permissive histone modifications.

Selective occupancy of human histone genes at the G_1/S-phase transition of the pluripotent cell cycle. The histone H4-specific transcription factor HINFP and RNA pol II are recruited in a temporal-spatial manner to the histone H4 gene during the shortened G_1 phase of pluripotent human ES and iPS cells. ChIP assays were performed using mitotically synchronized hES H9 cells that exhibit increased histone H4 and H3 and decreased cyclin E2 mRNA levels during progression from G_1 to early S phase (Fig. 4A). The association of RNA pol II with the histone H4 promoter and sequences downstream of the TSS increases in early S phase

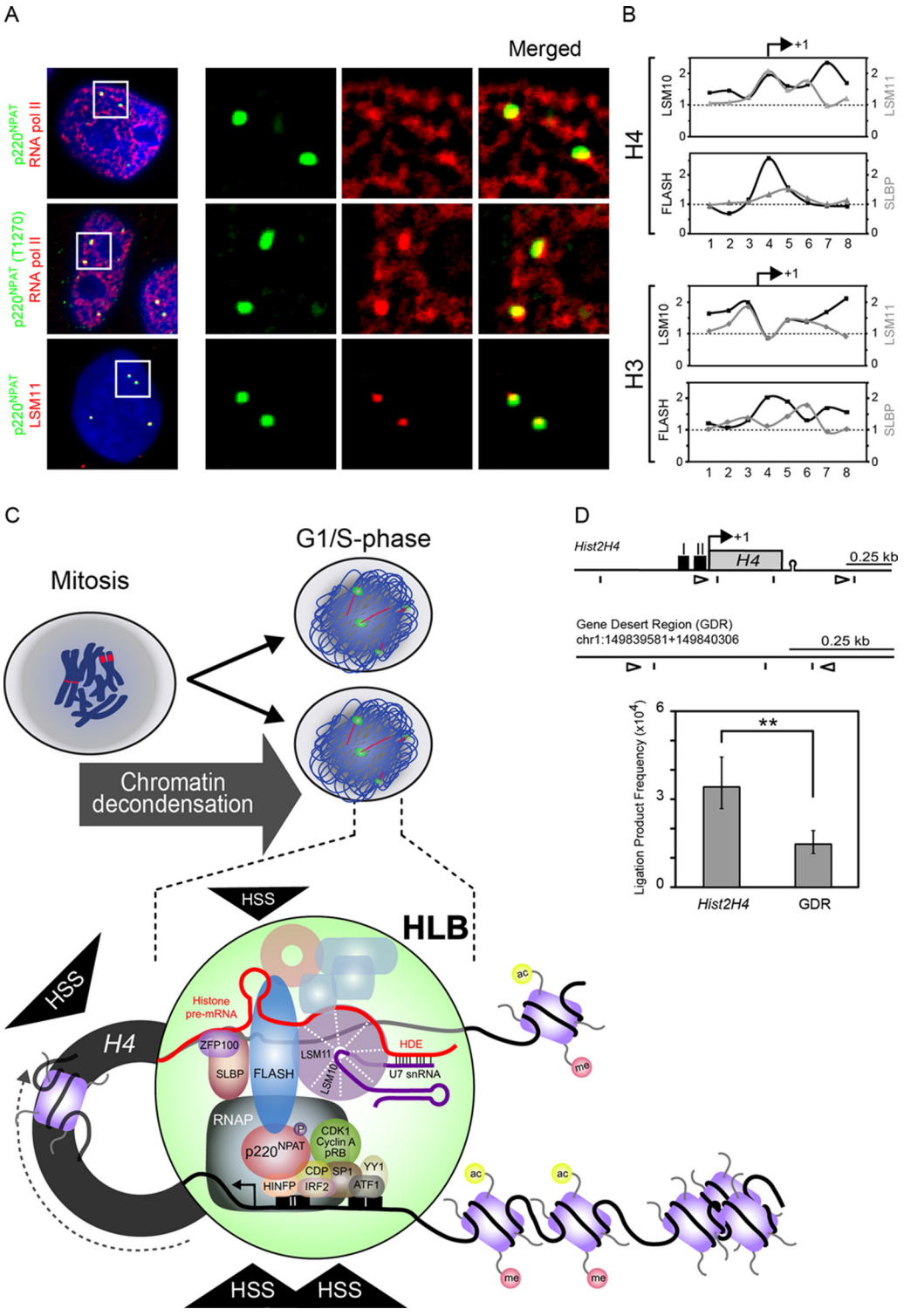

FIG 6 Molecular events associated with the activation and processing of human histone H4 transcripts. (A) Colocalization of 5′ and 3′ regulatory factors in hES cells. p220^{NPAT} foci (green) are associated with the transcriptional machinery (RNA pol II, top and middle panels, red) and 3′-end processing machinery (LSM11, lower panel, red) at histone gene clusters in human H9 cells. DAPI staining (blue) is used to visualize the nucleus. Panels on the right represent magnified images for each antibody and merged channels from the left panel (white squares). Merged images show that p220^{NPAT} foci, which denote HLBs, colocalize (yellow) with factors mediating histone pre-mRNA processing at sites of histone gene transcription. (B) Chromatin immunoprecipitation analysis of 3′-end-processing factors at H4 and H3 histone genes in human ES cells. Solid lines represent specific interactions above background IgG signal (dotted lines) of the 3′-end-processing factors LSM10 (black, top), FLASH (black, bottom), LSM11 (gray, top), and SLBP (gray, bottom) with the histone H4 and H3 genes. (C) Schematic representations of binding of histone H4-specific gene regulatory factors to sites I and II and binding of RNA pol II are shown (37, 38, 40, 57). Modifications of histone proteins upstream and downstream of the TSS and hypersensitivity to nucleases (HSSs; arrowheads) are also shown; nucleosomes located 1 kb upstream of the TSS are devoid of active histone modifications (unpublished observations). Several 3′-end-processing factors and proteins involved in transcription of the

(Fig. 4B, left panel). In contrast, HINFP binding is restricted to its recognition motif within site II upstream from the TSS in both G_1 and early S phase (Fig. 4B, left panel) and HINFP remains constitutively bound during the entire cell cycle of hES cells (Fig. 4C, left panel). Association of HINFP with the histone H4 gene was also observed throughout the cell cycle of synchronized WI-38 cells, though the signal was less pronounced than in hES cells (Fig. 4E, left panel). Strikingly, while HINFP binds constitutively, RNA pol II and $p220^{NPAT}$, which is the essential CDK2-responsive coactivator of HINFP, are both selectively recruited at the G_1/S transition and exhibit increased association during S phase in hES cells (Fig. 4C, left panel). Similarly, binding of RNA pol II to the histone H3 promoter and sequences downstream of the TSS mirrors those of the histone H4 at the G_1/S-phase transition (Fig. 4B, right panel) and during its maximal occupancy at mid-S phase (Fig. 4C, right panel). HINFP occupancy at the histone H3 locus is negligible throughout the cell cycle of hES cells, consistent with results from asynchronous cells (Fig. 3D). Temporal changes at the site of maximal occupancy within the histone H4 locus during the cell cycle of hES cells show that occupancy by RNA pol II and $p220^{NPAT}$ follows a remarkably similar pattern, peaking when histone H4 mRNA is at its highest level (Fig. 4D). Taken together, these data demonstrate that a dynamic and selective increase in protein-DNA interactions of the HINFP/$p220^{NPAT}$ coactivation complex and RNA pol II occurs during induction of histone H4 gene expression at the G_1/S-phase transition in hES cells.

Active epigenetic marks associate with histone genes during the cell cycle of hES cells. Epigenetic posttranslational modifications of histone proteins accompany cell cycle-dependent modulations in occupancy of RNA pol II and $p220^{NPAT}$ at the histone H4 promoter. ChIP analysis shows that covalent modifications of histone proteins associated with transcriptional activation (H3K4me3, H3K9ac) are present throughout the histone H4 locus with the exception of the region around the TSS, which is almost totally devoid of histone proteins (see, for example, total histone H3 in Fig. 5A). Strikingly, these same two epigenetic marks exhibit cell cycle-dependent changes both 5′ and 3′ of the histone H4 locus that begin in late G_1 phase and continue through S phase, concurrent with increased histone H4 expression (Fig. 5A). Other histone modifications that are normally associated with active transcription (H4K12ac and H4K16ac) are, as expected, preferentially detected in the distal 5′ region of the histone H4 promoter in hES cells (Fig. 5B) and show highly distinct temporal changes during the hES cell cycle. In contrast, the repressive epigenetic mark H3K27me3 is absent at the histone H4 locus in synchronized hES cells (Fig. 5B) yet is clearly detected at the *GATA6* and *OSX* loci that are not expressed (data not shown). The same dynamic posttranslational modifications of histone proteins are detected at the histone H3 locus at mid-S phase when maximal expression is observed (Fig. 5C and D).

We also analyzed epigenetic marks at the histone H4 locus during the cell cycle of normal fibroblasts, including H3K4me3, which shows a notably different pattern than that observed in asynchronous hES cells (Fig. 3B). ChIP analysis shows that high levels of the active marks H3K4me3 and H4K12ac are present throughout the histone H4 locus, including the regions around the TSS, coding sequences, and 3′ end (Fig. 5E and F). This pattern represents a remarkable difference from that observed in hES cells (Fig. 5A and B). As with hES cells, the repressive epigenetic mark H3K27me3 is absent at the histone H4 locus in synchronized WI-38 cells (Fig. 5F, bottom panel). The total histone H3 pattern in synchronized normal somatic cells also shows a major difference with hES cells (Fig. 5F, bottom panel), and data normalized to the total histone signal show a significant difference between hES (Fig. 5G) and WI-38 (Fig. 5H) cells at the histone H4 locus at mid-S phase when maximal expression is observed. Strikingly, in hES cells the region around the TSS is devoid of these covalent modifications, but in somatic cells these epigenetic marks remain unchanged throughout the gene locus. These results indicate that epigenetic marks for active chromatin at histone gene promoters support cell cycle-dependent changes in histone gene expression and occupancy of histone gene transcription factors in pluripotent hES cells.

Three-dimensional chromatin architecture of the transcriptionally active histone genes. The epigenetic changes that support stimulation of histone H4 gene transcription occur concomitant with the selective cell cycle-dependent recruitment of the CDK2/cyclin E responsive coactivator $p220^{NPAT}$ that interacts with the constitutively bound histone H4-specific transcription factor HINFP to mediate the association of RNA pol II with the histone H4 loci (26, 32, 37, 38, 40, 53, 57, 59, 61). Our model postulates that the 5′ and 3′ regions of the histone H4 locus interact through key HLB components that form a protein-protein bridge. To test our model, we performed immunofluorescence microscopy and ChIP assays with representative HLB components involved in 5′-related transcriptional functions and 3′-related processing functions (Fig. 6 and data not shown) (see also reference 15). Immunofluorescence microscopy shows that the transcriptional component $p220^{NPAT}$ colocalizes with both RNA pol II and the 3′-end processing factor LSM11 (Fig. 6A). Importantly, ChIP results indicate that 3′-related factors LSM10, LSM11, FLASH, and SLBP interact with both the histone promoter and the region encoding the 3′-end hairpin loop of the histone H4 and H3 mRNAs (Fig. 6B). We have also observed association of FLASH and SLBP with similar regions of the histone H4 locus in the glioblastoma cell line T98G (data not shown). Furthermore, using a proximity ligation assay (see Materials and Methods), we find a looping interaction between sequences upstream and downstream of the histone H4 gene. Restriction fragments containing the 5′ and the 3′ ends of the *HIST2H4* gene show a higher ligation frequency than that in a gene desert region near the histone gene (Fig. 6D). Thus, dynamic G_1/S-phase-related changes in protein-DNA interactions that occur within an intricate mi-

replication-dependent histones colocalize to specific subnuclear foci known as histone locus bodies (HLBs) (21, 22). FLASH protein also localizes to HLBs (7, 23), is required for transcription and 3′-end processing of histone mRNAs (2, 14, 28, 58), and interacts with histone gene loci (Fig. 6B and data not shown). The schematic representation of components involved in 3′-end processing of histone pre-mRNAs was adapted from that of Dominski with permission (15). (D) Proximity ligation assay of the *HIST2H4* gene. The top panel shows a schematic of the genomic organization of the human histone H4 gene and a gene desert region (GDR) near the histone H4 locus. The set of primers (open arrowheads) used for analyses and the FatI restriction sites (lines) are shown. The histone H4 locus (bottom panel) shows a higher ligation frequency than a gene desert region, indicating a looping interaction between the 5′ and 3′ ends of the histone H4 gene (**, $P < 0.01$).

croenvironment of active epigenetic marks and histone locus body components together support a transcriptionally active architectural chromatin configuration at the histone locus (Fig. 6C).

DISCUSSION

Pluripotent stem cells must remodel chromatin architecture during the cell cycle within a predominantly euchromatin background, in contrast to differentiated cells, where the genome is architecturally and functionally organized as a composite of euchromatin and gene-repressive heterochromatin. The accelerated G_1 phase of the cell cycle in hES cells demands rapid and selective chromatin remodeling of S-phase-specific genes. We have established that histone gene expression is the most prominent S-phase-related transcriptional program in pluripotent human embryonic stem (hES) cells, providing a paradigm for examining cell cycle-dependent modifications in chromatin architecture during self-renewal.

We show that dynamic gene regulatory interactions at the histone H4 locus in hES cells occur in an "open" chromatin environment reflected by a nucleosome-free hypersensitive region at the transcription start site (TSS) and an enrichment of active epigenetic histone marks throughout the promoter and coding sequences (e.g., H3K4me3, H3K9ac) or selectively enriched in the region upstream of the TSS (e.g., H4K12ac, H4K16ac). The entire histone H4 gene locus appears to be devoid of H3K27me3 modification, which marks transcriptionally inactive chromatin. The absence of H3K27me3 is consistent with the highly accessible chromatin conformation of the H4 gene that is evidenced by its pronounced nuclease sensitivity. A similar pattern of histone protein modifications was found for the histone H3 gene, suggesting that this is a general mechanism for histone genes in hES cells. Normally, active marks (e.g., H3K4me3, H3K9ac, H4K12ac, and H4K16ac) are preferentially associated with locations at the 5′ end of the gene, while here we find that these marks are also selectively enriched in the 3′ region of the H4 and H3 genes that encode sequences supporting mRNA maturation (Fig. 5 and 6). In contrast, in normal fibroblasts, besides a less pronounced association of RNA pol II and HINFP, relatively constant levels of active epigenetic marks (e.g., H3K4me3 and H3K9ac) are present throughout the histone H4 locus, thus indicating that a smaller fraction of WI-38 cells are progressing through S phase. Hence, in hES cells histone loci are distinctly organized in a hypersensitive configuration that renders the 5′ and 3′ regions of the gene highly accessible to the machinery required for transcript initiation and processing. The functional efficiency afforded by this unique chromatin topology may facilitate the accelerated G_1-phase progression in hES cells.

The activation of histone H4 gene expression at histone locus bodies occurs concomitant with constitutive binding of the histone H4-specific transcription factor HINFP and the selective cell cycle-dependent recruitment of the CDK2/cyclin E responsive coactivator $p220^{NPAT}$, which together mediate the association of RNA pol II (32, 37, 38, 40, 53, 57, 59, 61) with the histone H4 loci (Fig. 6). Furthermore, $p220^{NPAT}$ associates with FLASH, LSM11, and SLBP (2, 7, 23), indicating formation of a subnuclear macromolecular complex that supports both RNA transcript initiation and processing. Our ChIP data, as well as the published literature, indicate that selected HLB components bind to both 5′ and 3′ regions of the histone H4 locus (2, 14, 28, 58) (Fig. 6 and data not shown), thus potentially permitting a looped chromatin configuration that supports the rapid induction of histone gene expression at the G_1/S-phase transition in both human embryonic stem cells and induced pluripotent stem cells.

The accelerated G_1 phase of pluripotent (hES and iPS) cells imposes major temporal constraints on the remodeling of chromatin as cells mitotically divide and prepare for progression into S phase. As pluripotent cells globally decondense chromosome structure, selective accessibility to cell cycle-regulated genes must be retained within a chromatin context exhibiting limited heterochromatinization. This study reveals critical epigenetic parameters that govern the establishment of chromatin structure conducive for transcriptional induction of selected genomic loci at the G_1/S-phase transition. We find that the chromatin architecture of highly expressed genes encoding histone proteins, which are required for packaging of newly replicated DNA during S phase, is dynamically remodeled as cells progress rapidly from mitosis through G_1 into S phase. This active remodeling is accompanied by an orchestrated recruitment of key gene regulatory factors, the presence of a nucleosome-free region surrounding the TSS, and atypical epigenetic marking of nucleosomes. We conclude that self-renewal of pluripotent stem cells requires sequential reconfigurations of the genome in rapid succession after the completion of mitosis within a highly contracted G_1 phase—global chromatin decondensation immediately followed by the assembly of subnuclear microenvironments and the cell cycle stage-specific and gene-selective local remodeling of chromatin structure to support gene activation essential for S phase. Our study defines a novel architectural dimension to control gene expression for self-renewal of human pluripotent stem cells.

ACKNOWLEDGMENTS

We thank Judy Rask and Patricia Jamieson for expert assistance with manuscript preparation. We also thank Phyllis Spatrick, David Lapointe, Stephen Baker, and Mei Xu from UMMS for expert advice with microarray and statistical analysis and Wade Harper (Harvard Medical School), Zbigniew Dominski (University of North Carolina at Chapel Hill), Rudolf Jaenisch (The Whitehead Institute), and Vincenzo De Laurenzi (Universita G. d'Annunzio Chieti-Pescara) for generously providing antibodies and/or cell lines. We also thank the members of our research group and especially Kaleem Zaidi and Jason Dobson for stimulating discussions and Margaretha van der Deen for histone H4 primer (1, 2, 3, 5, and 6) sequences.

Studies reported were in part supported by National Institutes of Health grants RC1 AG035886-01 (to G.S.S. and A.J.V.W.) and R01 CA139322-03 (to G.S.S. and J.L.S.), as well as FONDECYT contract grant 1095075 (to M.M.) and FONDAP contract grant 15090007 (to M.M.).

The contents of this paper are solely the responsibility of the authors and do not necessarily represent the official views of the National Institutes of Health.

We declare no competing financial interests.

REFERENCES

1. **Ahmed K, et al.** 2010. Global chromatin architecture reflects pluripotency and lineage commitment in the early mouse embryo. PLoS One **5**:e10531. doi:10.1371/journal.pone.0010531.
2. **Barcaroli D, et al.** 2006. FLASH is required for histone transcription and S-phase progression. Proc. Natl. Acad. Sci. U. S. A. **103**:14808–14812.
3. **Becker KA, et al.** 2006. Self-renewal of human embryonic stem cells is supported by a shortened G1 cell cycle phase. J. Cell. Physiol. **209**:883–893.
4. **Becker KA, Stein JL, Lian JB, van Wijnen AJ, Stein GS.** 2007. Establishment of histone gene regulation and cell cycle checkpoint control in human embryonic stem cells. J. Cell. Physiol. **210**:517–526.

5. **Bilodeau S, Kagey MH, Frampton GM, Rahl PB, Young RA.** 2009. SetDB1 contributes to repression of genes encoding developmental regulators and maintenance of ES cell state. Genes Dev. **23**:2484–2489.
6. **Bond GL, Hu W, Levine AJ.** 2005. MDM2 is a central node in the p53 pathway: 12 years and counting. Curr. Cancer Drug Targets **5**:3–8.
7. **Bongiorno-Borbone L, et al.** 2008. FLASH and NPAT positive but not coilin positive Cajal bodies correlate with cell ploidy. Cell Cycle **7**:2357–2367.
8. **Boyer LA, et al.** 2005. Core transcriptional regulatory circuitry in human embryonic stem cells. Cell **122**:947–956.
9. **Boyer LA, et al.** 2006. Polycomb complexes repress developmental regulators in murine embryonic stem cells. Nature **441**:349–353.
10. **Chen X, et al.** 2008. Integration of external signaling pathways with the core transcriptional network in embryonic stem cells. Cell **133**:1106–1117.
11. **Cole MF, Young RA.** 2008. Mapping key features of transcriptional regulatory circuitry in embryonic stem cells. Cold Spring Harbor Symp. Quant. Biol. **73**:183–193.
12. **Corbeil RR, Searle SR.** 1976. Restricted maximum likelihood (REML) estimation of variance components in the mixed model. Technometrics **18**:31–38.
13. **Daniel WW.** 1990. Applied nonparametric statistics. Duxbury, Pacific Grove, CA.
14. **De Cola A, et al.** 2012. FLASH is essential during early embryogenesis and cooperates with p73 to regulate histone gene transcription. Oncogene **31**:573–582.
15. **Dominski Z.** 2010. An RNA end tied to the cell cycle: new ties to apoptosis and microRNA formation? Cell Cycle **9**:1308–1312.
16. **Efroni S, et al.** 2008. Global transcription in pluripotent embryonic stem cells. Cell Stem Cell **2**:437–447.
17. **Erkmann JA, et al.** 2005. Nuclear import of the stem-loop binding protein and localization during the cell cycle. Mol. Biol. Cell **16**:2960–2971.
18. **Feng Z, Hu W, Rajagopal G, Levine AJ.** 2008. The tumor suppressor p53: cancer and aging. Cell Cycle **7**:842–847.
19. **Freedman DA, Wu L, Levine AJ.** 1999. Functions of the MDM2 oncoprotein. Cell. Mol. Life Sci. **55**:96–107.
20. **Gaspar-Maia A, et al.** 2009. Chd1 regulates open chromatin and pluripotency of embryonic stem cells. Nature **460**:863–868.
21. **Ghule PN, et al.** 2007. Cell cycle dependent phosphorylation and subnuclear organization of the histone gene regulator $p220^{NPAT}$ in human embryonic stem cells. J. Cell. Physiol. **213**:9–17.
22. **Ghule PN, et al.** 2009. The subnuclear organization of histone gene regulatory proteins and 3′ end processing factors of normal somatic and embryonic stem cells is compromised in selected human cancer cell types. J. Cell. Physiol. **220**:129–135.
23. **Ghule PN, et al.** 2008. Staged assembly of histone gene expression machinery at subnuclear foci in the abbreviated cell cycle of human embryonic stem cells. Proc. Natl. Acad. Sci. U. S. A. **105**:16964–16969.
24. **Ghule PN, et al.** 2011. Reprogramming the pluripotent cell cycle: restoration of an abbreviated G1 phase in human induced pluripotent stem (iPS) cells. J. Cell. Physiol. **226**:1149–1156.
25. **Hockemeyer D, et al.** 2008. A drug-inducible system for direct reprogramming of human somatic cells to pluripotency. Cell Stem Cell **3**:346–353.
26. **Holmes WF, et al.** 2005. Coordinate control and selective expression of the full complement of replication-dependent histone H4 genes in normal and cancer cells. J. Biol. Chem. **280**:37400–37407.
27. **Hovhannisyan H, et al.** 2003. Maintenance of open chromatin and selective genomic occupancy at the cell-cycle-regulated histone H4 promoter during differentiation of HL-60 promyelocytic leukemia cells. Mol. Cell. Biol. **23**:1460–1469.
28. **Kiriyama M, Kobayashi Y, Saito M, Ishikawa F, Yonehara S.** 2009. Interaction of FLASH with arsenite resistance protein 2 is involved in cell cycle progression at S phase. Mol. Cell. Biol. **29**:4729–4741.
29. **Lee TI, et al.** 2006. Control of developmental regulators by Polycomb in human embryonic stem cells. Cell **125**:301–313.
30. **Levine AJ.** 1997. p53, the cellular gatekeeper for growth and division. Cell **88**:323–331.
31. **Loh YH, et al.** 2006. The Oct4 and Nanog transcription network regulates pluripotency in mouse embryonic stem cells. Nat. Genet. **38**:431–440.
32. **Ma T, et al.** 2000. Cell cycle-regulated phosphorylation of p220(NPAT) by cyclin E/Cdk2 in Cajal bodies promotes histone gene transcription. Genes Dev. **14**:2298–2313.
33. **Maherali N, et al.** 2007. Directly reprogrammed fibroblasts show global epigenetic remodeling and widespread tissue contribution. Cell Stem Cell **1**:55–70.
34. **Marson A, et al.** 2008. Connecting microRNA genes to the core transcriptional regulatory circuitry of embryonic stem cells. Cell **134**:521–533.
35. **Mattout A, Meshorer E.** 2010. Chromatin plasticity and genome organization in pluripotent embryonic stem cells. Curr. Opin. Cell Biol. **22**:334–341.
36. **McLean RA, Sanders WL, Stroup WW.** 1991. A unified approach to mixed linear models. Am. Stat. **45**:54–64.
37. **Medina R, van Wijnen AJ, Stein GS, Stein JL.** 2006. The histone gene transcription factor HiNF-P stabilizes its cell cycle regulatory co-activator $p220^{NPAT}$. Biochemistry **45**:15915–15920.
38. **Miele A, et al.** 2005. HiNF-P directly links the cyclin E/CDK1/$p220^{NPAT}$ pathway to histone H4 gene regulation at the G_1/S phase cell cycle transition. Mol. Cell. Biol. **25**:6140–6153.
39. **Miele A, Dekker J.** 2009. Mapping cis- and trans- chromatin interaction networks using chromosome conformation capture (3C). Methods Mol. Biol. **464**:105–121.
40. **Mitra P, et al.** 2003. Identification of HiNF-P, a key activator of cell cycle-controlled histone H4 genes at the onset of S phase. Mol. Cell. Biol. **23**:8110–8123.
41. **Moreno ML, Chrysogelos SA, Stein GS, Stein JL.** 1986. Reversible changes in the nucleosomal organization of a human H4 histone gene during the cell cycle. Biochemistry **25**:5364–5370.
42. **Okita K, Ichisaka T, Yamanaka S.** 2007. Generation of germline-competent induced pluripotent stem cells. Nature **448**:313–317.
43. **Pardee AB.** 1974. A restriction point for control of normal animal cell proliferation. Proc. Natl. Acad. Sci. U. S. A. **71**:1286–1290.
44. **Pardee AB.** 1989. G1 events and regulation of cell proliferation. Science **246**:603–608.
45. **Park IH, et al.** 2008. Reprogramming of human somatic cells to pluripotency with defined factors. Nature **451**:141–146.
46. **Pasini D, et al.** 2008. Regulation of stem cell differentiation by histone methyltransferases and demethylases. Cold Spring Harbor Symp. Quant. Biol. **73**:253–263.
47. **Pillai RS, et al.** 2003. Unique Sm core structure of U7 snRNPs: assembly by a specialized SMN complex and the role of a new component, Lsm11, in histone RNA processing. Genes Dev. **17**:2321–2333.
48. **SAS Institute Inc.** 1997. The MIXED procedure, p 571–702. *In* SAS/STAT software: changes and enhancements through release 6.12, 1st ed. SAS Institute, Inc., Cary, NC.
49. **Schaniel C, et al.** 2009. Smarcc1/Baf155 couples self-renewal gene repression with changes in chromatin structure in mouse embryonic stem cells. Stem Cells **27**:2979–2991.
50. **Silva J, Smith A.** 2008. Capturing pluripotency. Cell **132**:532–536.
51. **Takahashi K, et al.** 2007. Induction of pluripotent stem cells from adult human fibroblasts by defined factors. Cell **131**:861–872.
52. **Takahashi K, Yamanaka S.** 2006. Induction of pluripotent stem cells from mouse embryonic and adult fibroblast cultures by defined factors. Cell **126**:663–676.
53. **Wei Y, Jin J, Harper JW.** 2003. The cyclin E/Cdk2 substrate and Cajal body component p220(NPAT) activates histone transcription through a novel LisH-like domain. Mol. Cell. Biol. **23**:3669–3680.
54. **Wernig M, et al.** 2007. In vitro reprogramming of fibroblasts into a pluripotent ES-cell-like state. Nature **448**:318–324.
55. **Winer BJ.** 1971. Statistical principles in experimental design. McGraw-Hill Book Company, New York, NY.
56. **Workman JL, Kingston RE.** 1998. Alteration of nucleosome structure as a mechanism of transcriptional regulation. Annu. Rev. Biochem. **67**:545–579.
57. **Xie R, et al.** 2009. The histone gene activator HINFP is a non-redundant cyclin E/CDK2 effector during early embryonic cell cycles. Proc. Natl. Acad. Sci. U. S. A. **106**:12359–12364.
58. **Yang XC, Burch BD, Yan Y, Marzluff WF, Dominski Z.** 2009. FLASH, a proapoptotic protein involved in activation of caspase-8, is essential for 3′ end processing of histone pre-mRNAs. Mol. Cell **36**:267–278.
59. **Ye X, Wei Y, Nalepa G, Harper JW.** 2003. The cyclin E/Cdk2 substrate $p220^{NPAT}$ is required for S-phase entry, histone gene expression, and Cajal body maintenance in human somatic cells. Mol. Cell. Biol. **23**:8586–8600.
60. **Yu J, et al.** 2007. Induced pluripotent stem cell lines derived from human somatic cells. Science **318**:1917–1920.
61. **Zhao J, et al.** 2000. NPAT links cyclin E-Cdk2 to the regulation of replication-dependent histone gene transcription. Genes Dev. **14**:2283–2297.